

Experimental determination of local-bonding configuration at the early stages of growth of the heterogeneous Pt/InP(110) interface by synchrotron-radiation spectroscopy

P. Claverie, B. Carriere,* R. Pinchaux,[†] and G. Rossi

Laboratoire pour l'Utilisation du Rayonnement Electromagnetique, Université de Paris-Sud, F-94305 Orsay, France

(Received 9 June 1986; revised manuscript received 15 January 1988)

The interaction of Pt adatoms with the InP(110) cleaved surface for coverages between 0.1 and 6 monolayers (ML) is studied to explore the chemical-bonding configuration at the early stages of formation of the interface. The Pt/InP(110) interface is heterogeneous: a dominant reacted Pt-P phase forms on patches of surface and grows in depth; traces of other Pt minority environments are observed; regions of the InP surface remain unreacted; and In is segregated. The Cooper-minimum photoemission method, using synchrotron radiation as the photon source, is employed to obtain indicators of the partial density of states of Pt *5d* character and P *3sp* character of the Pt-P dominant reacted phase. Core-level synchrotron-radiation photoelectron spectroscopy (Pt *4f*, In *4d*, P *2p*) and P *L*_{2,3} *VV* Auger line-shape results are also presented. The bonding structure between Pt and P at the interface formed by 3 and 6 monolayers of Pt on InP(110) is reminiscent of the Pt silicides.

INTRODUCTION

Heterogeneity of metal-semiconductor interfaces is a general phenomenon in the early stages of growth of the junction, in particular for interfaces on compound semiconductors.¹⁻³ The improvements of the resolution and the better signal-to-noise ratio of recent data have allowed one to recognize more components in the core-level signals from interfaces and to sketch the evolution of the associated chemical environments as a function of the interface growth, i.e., as a function of metal coverage and kinetic conditions. A variety of growth modes in the submonolayer and monolayer regime have been proposed: formation of microclusters of adsorbed metal at the semiconductor surface; catalytic action of the clusters on the chemical reaction between adsorbate and substrate; phase separation of reacted islands onto unreacted substrates, or onto substrates stabilized by a chemisorbed monolayer; etc. All such interfaces are spatially heterogeneous, with the substrate being partially covered by clusters or two-dimensional films (often called rafts) or locally reacted in depth with formation of islands (let us call them icebergs) of a reacted phase. The study of these systems demands the use of space-resolved physical probes like scanning electron tunneling microscopy and spectroscopy⁴ or spatially resolved Auger line-shape spectroscopy.⁵

We present in this paper the first synchrotron-radiation photoemission study of the growth of the Pt/InP(110) interface at room temperature. It is shown the heterogeneous character of this system for low coverages and the tunability of the photoemission parameters are exploited in order to analyze the chemical nature of the main reacted interface phase. This is possible since one well-defined chemical environment for the adsorbed Pt is found, and since the favorable ratio of photoionization cross sections for the valence-electron states of the interface atoms allows the exploitation of the Cooper-minimum effect. The

experimental basis of the discussion is provided by Pt *4f*, In *4d*, P *2p* core photoemission, P *L*_{2,3} *VV* Auger line-shape measurement, valence-band photoemission and Cooper-minimum photoemission, and measurement of the magnitude of the Cooper minimum effect on the photoionization cross section of the atomiclike In *4d* subshell, and of the bandlike Pt *5d* subshell. By choosing the proper photoexcitation energies we have obtained the angular-momentum-dependent density of states (or partial DOS, PDOS) and other information on the initial-state wave functions.⁶⁻⁸

EXPERIMENT

Two series of measurements were done, following the same sample-preparation procedures on two different synchrotron-radiation ports outputting monochromatic radiation in the photon energy ranges 20–50 eV and 80–180 eV, on the ACO storage ring at LURE. The experiments were done using two ultrahigh-vacuum apparatuses equipped with hemispherical electrostatic electron energy and angular distribution analyzers as well as LEED, Auger, and standard sample-preparation techniques. InP(110) surfaces were obtained from *n*-type single-crystal rods by cleavage *in situ*. Pt was evaporated from 99.995% pure Pt wires wrapped around a W filament heated Ohmically. The deposition rate was monitored by a quartz microbalance that could be put in the target position alternatively with the sample. The control of stable evaporation rates was quite laborious due to slow thermal drifts of the quartz microbalance; the overall accuracy of the coverages is $\pm 30\%$. The thermal drifts of the quartz microbalance are a qualitative indication of warming of the substrate surface during Pt evaporation. The photoemission measurements were done with the photon beam impinging on the sample at 22.5° with respect to the surface normal; the photoelectrons were collected at normal emission and at 20° along the [110] direction.^{9,10}

THE COOPER-MINIMUM METHOD

A feature of synchrotron-radiation spectroscopy is the access to the photoionization cross-section parameter $\sigma(h\nu)$ in the photoexcitation process.¹¹ By changing the photon energy within the excitation range of interest for surface-sensitive photoelectron spectroscopy of valence states (20–200 eV) it is possible to distinguish the different orbital contributions to the total density of states when the relative variations of the photoionization cross sections among those states are large. A noteworthy case, already discussed in the literature, is that of the *4d* and *5d* valence-band states in the metals of the second and third transition period.^{6,7,12} The photoionization cross section for *4d* and *5d* states is very large at the lower end of the surface-sensitive spectroscopy range (relative to *sp* states) but is strongly reduced at the Cooper minimum, close to the upper end of that energy range (150–200 eV).

We briefly recall in the following the method which is then applied to the Pt/InP(110) data in the following section. The photoelectron signal is measured as a current or count rate $C(h\nu)$ which was previously⁶ parametrized as

$$C(h\nu) \propto \sigma(h\nu)L(E')\Gamma(E_K)\Phi(h\nu)F(X,n,K,L),$$

where $\sigma(h\nu)$ is the photoionization cross section, $L(E')$ is the escape depth for the photoelectron of final-state energy E' , $\Gamma(E_K)$ is the efficiency of the electron analyzer for photoelectrons of kinetic energy E_K , $\Phi(h\nu)$ is the photon flux (throughout of the monochromator), and $F(X,n,K,L)$ is a factor that takes into account all the optical effects which are dependent upon the photon wavelength and photoelectron wavelength (reflection and refraction as a function of the angle of incidence X , index of refraction $n + iK$, and L).^{6,13} It is possible to set the experimental conditions such as to minimize the $h\nu$ -dependent variations of the optical effects (for example, by working at near-normal photon incidence),¹³ and to gauge the escape depth and analyzer-efficiency factors by means of a core-level photoemission standard [deep core levels are assumed to follow atomiclike $\sigma(h\nu)$].¹⁴ The reference cross-section values calculated in the Hartree-Fock-Slater (HFS) approximation are tabulated for the external subshells of all elements.¹⁵ It has been shown⁶ that the photoionization cross sections are sensitive to the hybridization of the orbitals so that the atomic cross-section values can only be used as qualitative indicators of the relative order of magnitude and overall photon energy dependence of valence-band states.

Table I summarizes the relative sensitivity values, as derived from the atomic cross sections for the Pt/InP system.¹⁵ The relative weight of the photoemission originating from Pt *5d* states and InP *3sp* states is such that at $h\nu=25$ eV, Pt *5d* is expected to dominate by a factor of 40 the other contributions, at $h\nu=80$ eV by a factor of 4.5, and at the Cooper minimum ($h\nu=160$ eV) it is the InP *3sp* intensity that is expected to dominate by a factor of 2 the Pt photoemission in the spectra. The solid-state value of the Pt *5d* cross-section reduction at the Cooper minimum is probably different from the atomic calculations. As a reference we use the fact that the Au *5d* pho-

TABLE I. Indicators of the relative spectral weight of the orbital components of the valence-band states at the Pt/InP(110) interface for the photon energy values used in the experiment in the atomic orbitals approximation. These relative values are derived from the atomic Hartree-Slater calculations of the photoionization cross section tabulated in Ref. 15.

Orbital	25 eV	80 eV	160 eV
In 5s	0.32%	2.1%	8.5%
P 3s	0.98%	6.4%	22.4%
P 3p	1.25%	10%	35%
Pt 5d	97.5%	81%	32%
Pt 6s	0.05%	0.5%	2.1%

toionization cross section at the Au/Si(111) interface and at the Au/InP(110) interface (both interfaces form as a random alloy for coverages of the order of 5 ML, with low Au-Au coordination, and therefore small *5d-5d* overlap) shows a stronger Cooper-minimum effect, than for pure fcc Au.¹⁰ A system more similar to the one studied here from the chemical point of view is the Pd/Si(111), where the Pd *4d* valence states are hybridized with the ligand (Si) *3sp* states. In this case the depth of the cross-section minimum is slightly reduced with respect to the metallic fcc Pd case.⁶ Although the Cooper-minimum experimental data base is still limited, and it is difficult to generalize cross-section trends, we propose that (1) it is possible from the photoelectron spectra of the Pt/InP(110) interface to recognize the peaks of different orbital character, simply by comparing the relative intensity variations of the peaks as a function of $h\nu$; (2) it is possible to make difference curves of the experimental Pt/InP(110) spectra, such that one orbital contribution is emphasized, i.e., it is possible to obtain empirical indicators of the energy distribution of the partial density of states (PDOS) of Pt *5d* character and of P *3sp*.

RESULTS

The EDC's for Pt submonolayers on InP(110) of Fig. 1 were obtained with $h\nu=25$ eV photon energy and photoelectron analysis at 20° off normal in order to observe the P-associated surface state (called A_5 in the literature⁹) as a function of adsorbate abundance. A reduction of the surface-state peak intensity versus Pt coverage is observed, while the growing emission in the region between 2 and 6 eV below E_F shows the broad energy distribution of the Pt-induced valence states. The spectra in the figure have been aligned with respect to the P surface-state position in order to compare the shapes and to obtain the difference curve showing the distribution of the new states induced by the presence of submonolayers of Pt. The actual value of the energy shift of the InP valence-band maximum depended on the cleavage, being typically of the 0.7 ± 0.15 eV, a value also found in the Pd/*n*-type InP(110) system,¹⁶ smaller than 0.83 ± 0.1 eV in Pt/*n*-type GaAs(110).¹⁷ The normal-emission EDC's for coverages between 1 and 6 ML are summarized in Fig. 2. At 25 eV (and 50 eV, not shown) the spectra are dominat-

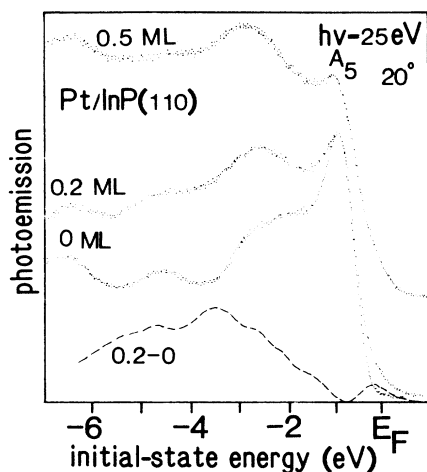


FIG. 1. Angular resolved electron-energy-distribution curves (EDC's) measured at 20° off normal in the $[110]$ direction to enhance the sensitivity to the $P A_5$ surface state. The bottom curve corresponds to the clean-InP(110) surface, but has been shifted by the Schottky barrier value (see text) in order to align the surface-state peak with the curves for 0.2 and 0.5 monolayers of Pt on InP(110). The dashed curve is the difference between the 0.2 and the clean (shifted) InP. It is representative of the distribution of the interface states.

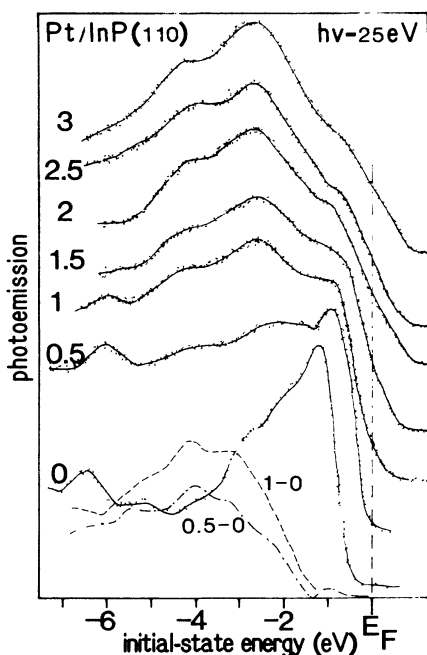


FIG. 2. Photoelectron EDC's excited with $h\nu=25$ eV and measured at normal emission for clean-InP(110) and Pt coverages as indicated. The dashed and dot-dashed curves represent the difference spectra between the 0.5 and 1 ML curves and the clean (energy shifted of the Schottky barrier value) curve. The Pt derived states are spread over a wide energy range.

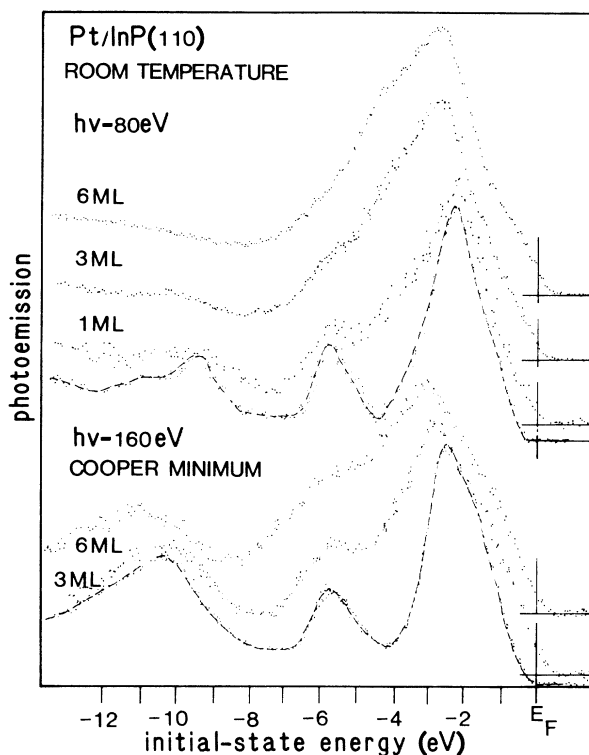


FIG. 3. Normal emission EDC's obtained with $h\nu=80$ eV and at the Cooper minimum ($h\nu=160$ eV) for cleaved InP(110) (dashed curves) and for Pt coverages onto InP(110). These spectra allow the experimental derivation of the d -like PDOS and p -like PDOS at the interface, as detailed in Figs. 5 and 6.

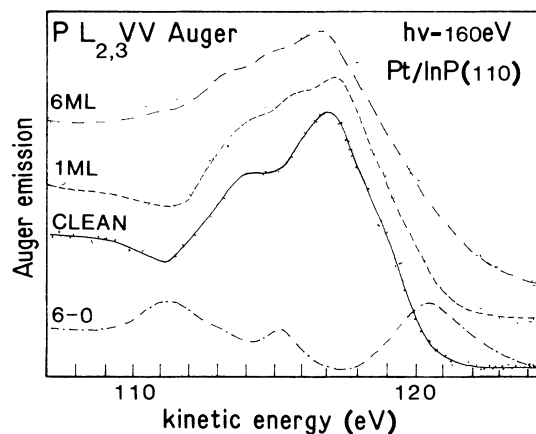


FIG. 4. Auger $P L_{2,3}VV$ line shapes as measured with $h\nu=160$ eV excitation, for clean InP(110) (solid curve), and for 1 ML Pt/InP(110) and for 6 ML Pt/InP(110). The dot-dashed curve at the bottom is the difference curve between the 6 ML and the clean spectra. A three-peaked structure is obtained with the three peaks being separated by ~ 4.5 eV similarly to the peaks of $3s$, $3p$ bonding and $3p$ antibonding states in the hybridized valence-band DOS.

ed by the Pt $5d$ derived photoemission which is peaked around 2.7 eV below E_F , and broadens almost symmetrically towards E_F and towards higher-binding energies. The shoulder due to the top of the InP valence band is still visible at 1 ML but it is progressively reduced in relative intensity whilst new states appear close to the Fermi level. Deep InP valence-band features are visible in the 1 ML spectrum obtained with $h\nu=80$ eV (Fig. 3), while the spectra obtained at higher coverages strongly resemble in shape and energy distribution the structures in the spectra obtained in angular integrated PES, at the same photon energy, for similar Pt coverages onto Si(111).¹⁸ The Cooper minimum EDC's are shown in Fig. 3. Figure 4 contains the P $L_{2,3}VV$ spectra obtained in the photoemission mode with $h\nu=160$ eV for 3 and 6 ML, showing the variations of the P $3sp$ states. The core photoemission spectra are shown in Fig. 5 (P $2p$), Fig. 6 (In $4d$), and Fig.

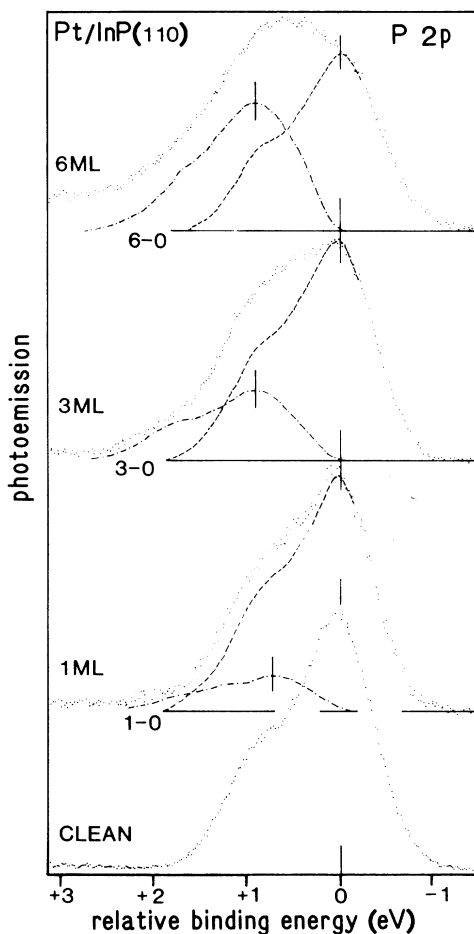


FIG. 5. P $2p$ core-level photoemission spectra for the clean-InP(110) surface, and for 1, 3, and 6 Pt monolayers on InP(110). The spectra have been aligned on the lowest-binding-energy edge and subtraction between the interface spectra and the clean substrate spectrum are shown as dot-dashed curves. The subtraction results show a single extra P $2p$ doublet, shifted by 0.85 ± 0.1 eV towards higher binding energies in the case of 3 and 6 ML. The chemical shift at 1 ML is 0.55 ± 0.1 eV.

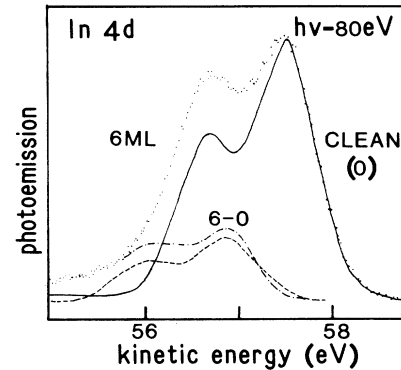


FIG. 6. In $4d$ core levels spectrum for 6 ML Pt/InP(110) (dots). The line shape of In $4d$ from cleaved InP(110) (solid line) is shifted to match the lower energy edge of the interface In $4d$ signal. The difference between the two spectra show a single extra doublet (dot-dashed). A second In $4d$ line shape from clean InP (dashed) is compared to the difference curve. The higher intensity in the high-energy tail of the interface spectrum can be attributed to a Sunjic-Doniach effect due to the metallic character of at least one of the In environments at the 6 ML interface (on this point the peak decomposition procedure is intrinsically ambiguous). The main component of the In $4d$ emission is shifted by 0.7 ± 0.1 eV towards lower-binding energies, i.e., towards a bulk-In binding energy, this is likely to be the metallic-In phase. The same result is obtained for 3 ML Pt/InP(110).

7 (Pt $4f$) with an empirical decomposition of the line shapes. The core photoemission line-shape decomposition has been obtained by aligning the component that represents the unreacted part of the core-level peaks with the clean line shape and making the difference curves, i.e., disregarding the presence of the unresolved surface-atom component in the clean InP(110) spectra. The core photoemission difference curves are compared in shape and intensity with the clean line shapes and are interpreted

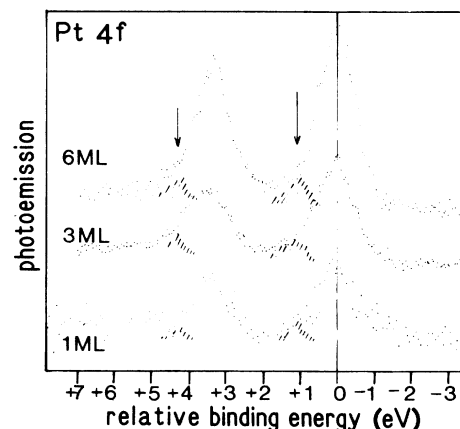


FIG. 7. Pt $4f$ core-level photoemission as a function of the Pt coverage. The spectra are aligned at the $4f_{7/2}$ peak; the minority doublet at 1 eV higher energy is shown by the dashed areas.

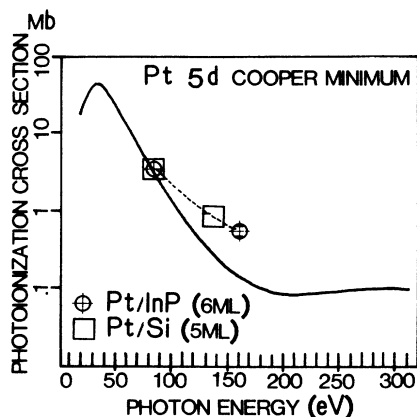


FIG. 8. Cooper-minimum curve of the photoionization cross section of the Pt 5d subshell. The solid curve represents the Hartree-Fock-Slater calculation of Ref. 15. The experimental data for reacted Pt/Si (Ref. 19) and Pt/InP interfaces are arbitrarily normalized at the $h\nu=80$ eV value to the theoretical atomic value. This allows to observe the reduction of the magnitude of the CM effect for the hybridized Pt 5d states of the interface compounds with respect to the localized Pt 5d atomic states.

ed as representative of chemically shifted spectra from the interface atoms. This procedure is fully empirical (no theoretical line shapes or fitting procedures are used); it relies on the assumption that the peak shape and the relative spin-orbit branching ratio should be basically unchanged for such deep core levels, a part of high-energy tails due to the metallic environment. The relevant information derived with this procedure are the relative binding energy and amplitude of the multicomponent peaks. It follows from this analysis that P is found at the interface in two environments, here called two phases, InP and Pt-P (Fig. 5). Indium is found in two environments too: InP and segregated In (Fig. 6). Most of the Pt 4f intensity is found in one doublet which defines the existence of one dominant environment for the Pt at the interface, with binding energy changes related to the coverage; a minority Pt 4f component at ~ 1 eV higher binding energy is also found. Its intensity is $< 15\%$ of the main doublet at 1 ML and $< 10\%$ at 6 ML (Fig. 7). From the attenuation of the P and In signal at 3 and 6 ML, and assuming an unchanged photoelectron-escape depth, we estimate that Pt atoms represent more than 50% of the material in the top layers of the interface.

The value of the CM effect for the Pt 5d states at the interface is plotted along with the atomic HFS cross section and with the Pt-Si reference data in Fig. 8.

DISCUSSION

The chemisorption stage of Pt at submonolayer coverage is characterized by a distribution of density of states between -2 and -6 eV below E_F , a small density-of-states peak close to E_F , and the partial survival of the clean InP(110) surface state A_5 associated to surface P

atoms, as well as the survival of the deep InP DOS peak mostly of P 3s character (not shown). The Pt 4f data for 1 ML show a main doublet with tails towards higher-binding energy. The presence of a minority site ($\leq 15\%$ of the Pt 4f signal in the main doublet at 1 ML) at the submonolayer stage could be compatible with Pt semi-isolated atoms or atoms with lower coordination number with the substrate, since the higher core-level binding energy with respect to the majority Pt and the weakness of the DOS peak close to E_F disfavor the interpretation in terms of Pt clustering.

The heterogeneity of the Pt/InP(110) interface becomes evident for the higher coverages. The P 2p line shapes of Fig. 5 are composed with a clean doublet that we attribute to patches of the surface unaffected by the presence of Pt and with a second doublet which is shifted towards higher-binding energies by 0.55 ± 0.2 eV for 1-ML Pt and by 0.85 ± 0.1 eV for 3 and 6 ML. The second doublet is well recognized if a clean P 2p line shape [from InP(110)] is reduced in amplitude and shifted in energy to fit the lowest binding energy edge of the P 2p line shape from the interface. This P 2p signal is associated with P which remains in the ionic environment. The difference curve (interface P 2p line shape minus clean-InP P 2p line shape) is then obtained which represents the contribution to the P 2p emission from the P atoms involved in the chemistry of the interface. This procedure gives as a result a single energy-shifted interface doublet with a line shape (width, spin-orbit branching ratio) similar to that for clean InP, apart from some intensity on the high-energy side which indicates a local metallic character. Furthermore the binding-energy shift is identical for 3 and 6 ML, while the amount of reacted P increases with the total Pt coverage. These results point to the existence of one well-defined interface reacted phase involving P in nonionic bonds. The reacted phase starts forming at low coverages and coexists with unreacted surface and substrate regions. The smaller P 2p shift measured at 1 ML represents the precursor stage of formation of the Pt-P phase, with lower P-Pt coordination. The reacted P component represents 25% of the total P 2p intensity at 3 ML and 42% at 6 ML. The total P 2p intensity at 6 ML is reduced to less than one-half of the clean-InP(110) intensity. These results indicate a growth of the reacted phase in depth as well as laterally on the substrate, since the escape depth of the photoelectrons detected is of the order of $7-10$ Å, and only large surface or near surface areas of nonreacted InP can explain the strong residual ioniclike signal. The Pt 4f core photoemission for 3 and 6 ML shows one dominant doublet indicating that 90% of the Pt atoms are in the same chemical environment, i.e., form a well-defined reacted phase with P. The In 4d core-level intensity is strongly reduced at the interface (30% of the clean-InP signal for 6 ML). A weak-In 4d doublet is measured at the clean-InP value plus the Schottky barrier shift, and a more intense In 4d doublet is measured at 0.7 ± 0.1 eV lower binding energy than in InP and is attributed to In which is excluded from the ionic environment of InP and is accumulated near the surface. The large binding-energy shifts of P 2p ($+0.85 \pm 0.1$ eV) and In 4d (-0.7 ± 0.1 eV) correspond to the charge redistribution

between the ligands. The electronegativity difference between Pt and P is small and the Pt—P bonds imply only a small charge transfer like the Pt—Si bonds. Breaking the InP ionic bonds allows charge to shift back from P to In. The apparent change in the branching ratio of the In 4*d* doublet is largely explained by the presence of the unreacted InP doublet. The residual intensity in the high-energy tail is due to the secondary tail of the intense shifted In peak and to a Sunjic-Doniach many-body tail which indicates that the shifted In signal originates from a metallic phase containing In, possibly in the shape of clusters or rafts as it was suggested for similar data on other *d*-metal–InP systems.^{10,16,20}

The core-level data indicate therefore a multiphase interface: two species of P environments with comparable concentrations, one at energies typical of ionic-bonded InP, the other corresponding to a metallic environment; one dominant configuration for Pt involving 90% of the Pt atoms, two In environments, also corresponding to ionic and metallic bonding.

These are the ingredients of the Pt/InP(110) interface heterogeneity in a coverage range where other reactive interfaces converge towards a uniformly reacted overlayer. The quantitative interpretation of the core-level attenuation profiles is difficult if a space distribution model of the heterogeneity is sought. For example, the ionic-metallic ratios of the In and P environments are different, and combinations of Pt-P icebergs, In segregation, and intermixing must be assumed. Although the above-described photoemission data base cannot indicate a simple model of the interface, one clearly recognizes the presence of a well-defined Pt-rich Pt-P reacted phase as the main product of the interface reaction between Pt and the InP(110) surface. At 6 ML this phase accounts for 90% of the Pt and 42% of the P signals, i.e., roughly two-thirds of the material forming the top layers of the interface.

THE BONDING AT THE Pt-P PHASE

We propose in this section the analysis of the bonding configuration between P and Pt at the reacted Pt-P interface phase. The hypothesis for such analysis is that the valence-band DOS at 3 and 6 ML is dominated by the Pt 5*d* contribution from 90% of the Pt atoms which are bonded with P and correspond in the core-level spectroscopy to the main Pt 4*f* doublet and to the chemically shifted P 2*p* doublet.

The support of this hypothesis comes from the selective sensitivity to the Pt 5*d*, P 3*sp*, and In 5*s* that *hν*-dependent photoemission can yield, as discussed below, so that a qualitative distinction of the different contributions to the total-measured valence-band spectra is obtained.

The accuracy limit of such analysis comes from the presence of a minority (< 10%) Pt signal in the 4*f* intensity and from the hypothesis that the valence-band DOS of all of the P atoms which contribute to the ioniclike P 2*p* signal can be approximated by the P 3*sp* spectrum of clean InP. In spite of these drastic approximations, we believe that the analysis, on the qualitative level, is mean-

ingful and instructive.

If one considers the relative values of the photoionization cross sections $\sigma(h\nu)$ (as calculated for free atoms, and summarized in Table I) of the various electron orbitals contributing to the measured spectra one finds the following.

(a) In the spectra obtained with $h\nu=80$ eV the Pt 5*d* derived states represent 81% of the signal, whilst at $h\nu=160$ eV the P 3*sp* + In 5*s* states represent 66.5% of the total signal.

On this basis one can interpret the difference spectrum between the $h\nu=80$ eV EDC and the $h\nu=160$ eV EDC as representing the energy distribution of the partial 5*d* density of states at the interface (second panel of Fig. 9).

(b) The In 5*s* contribution represents only a very small intensity, furthermore the 5*s* DOS for metallic In is flat up to E_F , therefore the In contributions to the valence band can be disregarded from the analysis.

(c) The P 3*s* and 3*p* states represent 58% of the total signal in the CM spectra ($h\nu=160$ eV), it is therefore possible to subtract from the experimental CM EDC's the residual contribution of 5*d* states by scaling the above determined Pt 5*d* PDOS to the proper relative value (from Table I) and obtain, by subtraction, a difference spectrum that can be interpreted as representing the P 3*sp* partial density of states at the interface (third panel of Fig. 9).

(d) By applying the hypothesis above defined on the state distribution associated to the ionically bonded P atoms we obtain a final difference spectrum by scaling the intensity of the InP clean valence-band spectrum to the relative value of the P 2*p* ionic intensity and subtracting it from the total P 3*sp* PDOS.

As a result of this empirical decomposition of the spectra we obtain difference spectra that represent the Pt 5*d* PDOS and P 3*sp* PDOS distributions of the Pt-P reacted interface phase.

Care should be taken in examining these difference spectra since their amplitudes are affected by the systematic errors intrinsic in the adoption of atomic cross sections and due to the unknown depth distribution of this phase. Indeed the *shape* of the difference curves, i.e., the energy distribution of the associated PDOS is largely independent upon changes in the normalization factors. On this empirical basis we will discuss, in the following, the qualitative features of the bonding at the Pt-P phase.

The 5*d* PDOS shows a prominent twin-peaked structure between -6 and -2 eV and a smaller peak close to E_F . The 5*d* PDOS of pure Pt on the contrary is highly asymmetric with the upper edge crossing the Fermi level and the main peak within -1 eV from E_F .¹⁸ The Pt 5*d* states at the interface are therefore heavily involved in the bonding with P, and the PDOS must be regarded as the density of mixed states of 5*d* character which are hybridized mostly with the P 3*p* state (the P 3*s* lie deeper in energy).

The counterpart of the *d*-band hybridization must be found in the P 3*sp* band PDOS. From the bottom panel of Fig. 9 it appears that the P valence states present a DOS peak around -10 eV which is attributed to a dominant 3*s* character, and a distribution of states of dom-

inant $3p$ character between -8 eV and the Fermi level. The P $3p$ PDOS of the reacted phase shows a broad structure between -8 and -3 eV with a peak at -3.6 eV, and a second weaker structure between -1.3 eV and E_F . The deeper part of the $3p$ PDOS does overlap with the deeper peak of the $5d$ PDOS. This leads to the attribution of this energy region to the density of bonding states formed by the hybridization of the Pt $5d$ -P $3p$ states. The DOS region close to E_F also shows peaks of both $5d$ PDOS and $3p$ PDOS. This could be associated to hybrid states of antibonding character, but the intensity of these features is small and must be considered with caution in these curves. It is noteworthy that a gap exists in the P $3p$ PDOS between ~ -2.6 and ~ -1.4 eV and that this gap corresponds to the shallower peak of the Pt $5d$ states, which can be interpreted as less involved in the rehybridization, in analogy with similar features in the DOS of Pt silicides.

An independent probe of the local P $3sp$ PDOS is represented by the line shape of the Auger $L_{2,3}VV$ transitions. The line shape of the reacted P for 6 ML (Fig. 4) shows three peaks with the two side peaks spaced by ~ 4.5 eV from the central one. These peaks correspond to the final-state Auger hole energy distribution in the bonding and antibonding P $3p$ PDOS and in the deep P $3s$ peak, which appear to be spaced by roughly 4.5 eV also in the photoemission spectra.^{10,16,21}

The description of the Pt-P states derived above is consistent with a bonding structure due to the hybridization of the Pt $5d$ and P $3p$ states with a relatively high-binding-energy peak of bonding states and possibly partial occupation of the antibonding states. More localized states are found at the bottom of the valence band, with P $3s$ character, and in the Pt $5d$ peak that corresponds to the energy gap between the bonding and the occupied antibonding states. The deep $3s$ -like structure is found

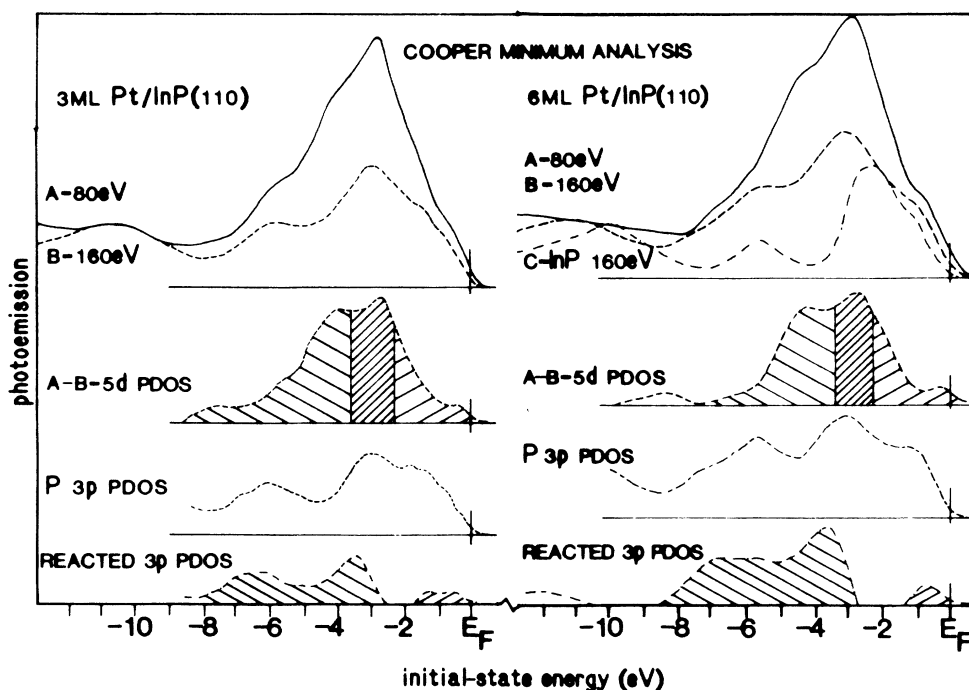


FIG. 9. Cooper-minimum analysis for the 3 ML (left panel) and 6 ML (right panel) Pt/InP(110) interface. The top (solid) curve in both panels is the EDC obtained with $h\nu=80$ eV, the dashed curve normalized to it at -11 eV is the Cooper-minimum curve obtained with $h\nu=160$ eV; the dot-dashed curve normalized at -11 eV, in the right panel, is the EDC for clean InP(110) as obtained with $h\nu=160$ eV. The second-level curves from the top down are the difference curves between the $h\nu=80$ eV and the Cooper-minimum spectra; they represent the d partial density of states. The central fine-dashed region is the region of the spectrum which undergoes the strongest Cooper-minimum effect (see Fig. 8). The third-level curves from the top down represent the Cooper-minimum curve reduced by the residual d contribution still present at the Cooper minimum, estimated according to Table I. The d contribution has been eliminated by subtracting the proper amount of the d PDOS line shape. This curve is an indicator of the averaged P $3sp$ PDOS at the interface, i.e., both from the ioniclike or unreacted InP and from the P-Pt phase. The bottom difference curves are indicators of the interface P-Pt PDOS of P $3p$ character: They are obtained by subtracting from the total P $3p$ DOS an amount of clean-InP(110) line shape which is calibrated by the relative weight of reacted-unreacted P $2p$ core-level photoemission peaks. By comparing the DOS peaks in the Pt $5d$ PDOS and P $3sp$ PDOS it is plausible to attribute the DOS features between -3 and -8 eV to bonding d - p hybrid states, and the DOS peaks between -2 and E_F to the partially occupied antibonding states. It is noteworthy that in correspondence with the more localized Pt $5d$ states, between -3.5 and -2.5 eV there is a gap (or a minimum) of P $3sp$ DOS.

shifted towards higher-binding energy by ~ 1 eV, indicating a broadening of the valence-band width at the interface with respect to pure InP.^{19,22}

CONCLUSIONS

The early stages of growth of the Pt/InP(110) interface consist in the formation of an heterogeneous system which presents the in top layers Pt-rich Pt-P phase probably growing in the form of icebergs, metallic In-rich regions, and ionic-bonded In and P. The bonding structure of the Pt-P phase is silicidelike with bonding-antibonding Pt $5d$ -P $3p$ molecular-orbital hybrid states. In spite of the high stability of this bonding structure, which is already present at coverages of the order of a monolayer, and grows consuming basically all of the Pt deposited at 3 and 6 ML, the Pt/InP(110) interface appears highly heterogeneous. It is noteworthy that the initial heterogeneity is maintained for coverages where the relative abundance of Pt is such that all of the P in the top region of the material could easily be converted from InP bonds to P-Pt bonds. It is possible that the presence of a metallic alloy phase containing In hinders the diffusion of Pt

to other extended regions of the substrate.

Further investigation in both the chemical analysis and space distribution of the Pt/InP(110) interface is needed in order to better characterize the minority interface phases that determine the heterogeneity. With this study we have also shown that the exploitation of the photoionization cross-section parameter in synchrotron radiation photoelectron spectroscopy allows one to investigate the electron states at heterogeneous interfaces: The measure of the partial density of states of a majority interface chemical environment involving $4d$ or $5d$ metals can be done with the Cooper-minimum method.

ACKNOWLEDGMENTS

Thanks are due to C. Guillot and D. Chaveau for assistance with one of the experiments. The experiments were done at the ACO storage ring at the Laboratoire pour l'Utilisation du Rayonnement Electromagnetique. LURE is supported by the CNRS, CEA, and MEN. The Laboratoire de Cristallographie is "unité associée au Centre National de la Recherche Scientifique" (U.A. No. 795).

*Present address: Laboratoire de Cristallographie, ULP Strasbourg, France.

†Present address: Université Pierre et Marie Curie, F-75005 Paris, France.

¹M. Grioni, J. Joyce, M. Del Giudice, D. G. O'Neill, and J. H. Weaver, *Phys. Rev. B* **30**, 7370 (1984).

²Y. Shapira, L. Brillson, A. J. Katnani, and G. Margaritondo, *Phys. Rev. B* **30**, 4586 (1984).

³I. Lindau, T. Kendelewicz, N. Newman, R. S. List, M. D. Williams, and W. E. Spicer, *Surf. Sci.* **162**, 591 (1985).

⁴F. Salvan, M. Fuchs, A. Baratoff, and G. Binnig, *Surf. Sci.* **162**, 634 (1985).

⁵L. Calliari, M. Sancrotti, and L. Braicovich, *Phys. Rev. B* **30**, 4885 (1984).

⁶G. Rossi, I. Lindau, L. Braicovich, and I. Abbati, *Phys. Rev. B* **28**, 3031 (1983).

⁷G. Rossi, in *Proceedings of the 17th International Conference on the Physics of Semiconductors*, edited by J. Chadi and W. Harrison (Springer-Verlag, New York, 1984), p. 149; Ph. D. thesis, Université Pierre et Marie Curie, Paris, 1985.

⁸L. Braicovich, *Surf. Sci.* **132**, 315 (1983).

⁹G. P. Srivastava, I. Singh, V. Montgomery, and R. H. Williams, *J. Phys. C* **16**, 3627 (1983).

¹⁰A. Barski, R. Pinchaux, and Giorgio Rossi, *Surf. Sci.* **154**, 629

(1985).

¹¹F. Bassani and M. Altarelli, in *Handbook on Synchrotron Radiation*, edited by E. E. Koch (North Holland, Amsterdam, 1983), Vol. I.

¹²I. Abbati, L. Braicovich, G. Rossi, I. Lindau, U. Del Pennino, and S. Nannarone, *Phys. Rev. Lett.* **50**, 1799 (1983).

¹³U. Del Pennino, S. Nannarone, I. Abbati, L. Braicovich, G. Rossi, and I. Lindau, *J. Electron Spectrosc. Relat. Phenom.* **37**, 389 (1986).

¹⁴M. H. Hecht, Ph. D. thesis, Stanford University, 1983.

¹⁵J. J. Yeh and I. Lindau, *At. Data Nucl. Data Tables* **32**, 1 (1985).

¹⁶T. Kendelewicz, W. G. Petro, I. Lindau, and W. E. Spicer, *Phys. Rev. B* **28**, 3618 (1983).

¹⁷C. E. McCants, T. Kendelewicz, K. A. Bertness, P. H. Mahowald, M. D. Williams, R. S. List, I. Lindau, and W. E. Spicer, *J. Vac. Sci. Technol. B* **5**, 1068 (1987).

¹⁸G. Rossi, I. Abbati, L. Braicovich, I. Lindau, and W. E. Spicer, *Phys. Rev. B* **25**, 3627 (1982).

¹⁹G. Rossi, *Surf. Sci. Rep.* **7**, 1 (1987).

²⁰T. Kendelewicz, G. Rossi, W. G. Petro, I. A. Babalola, I. Lindau, and W. E. Spicer, *J. Vac. Sci. Technol. B* **1**, 564 (1983).

²¹R. Weissman and K. Muller, *Surf. Sci. Rep.* **1**, 251 (1981).

²²C. Calandra, O. Bisi, and G. Ottaviani, *Surf. Sci. Rep.* **4**, 271 (1985).